



Cotransport of Suspended Colloids and Nanoparticles in Porous Media

G. V. C. Malgaresi¹ · H. Zhang¹ · C. V. Chrysikopoulos² · P. Bedrikovetsky¹

Received: 3 July 2018 / Accepted: 17 January 2019 / Published online: 5 February 2019
© Springer Nature B.V. 2019

Abstract

The objective of this study is to develop a model for cotransport of colloids and nanoparticles (NPs) in porous media under two particle capture mechanisms. The particle capture rate is proportional to the capture probability, which is a function of retained concentration, called the filtration function. Laboratory bench-scale experiments of individual transport of NPs and colloidal-size kaolinite clay particles through packed columns produced breakthrough curves (BTCs) that monotonically increased with time and stabilised at some value lower than the injected concentration. We discuss the filtration function that corresponds to BTCs stabilising at the concentration lower than the injected value. This so-called binary filtration function incorporates two particle capture mechanisms. The analytical transport model with a binary filtration function was capable to fit successfully BTCs obtained from individual transport experiments using kaolinite and NPs conducted by Chrysikopoulos et al. (Transp Porous Med 119(1):181–204, 2017). Assuming that the electrostatic particle–solid matrix interaction and the fraction of the solid matrix surface area occupied by a single attached particle (kaolinite or NP) are the same for individual transport of either kaolinite particles or NPs and for simultaneous cotransport of kaolinite particles and NPs, the proposed binary filtration function was extended for the cotransport case. Although the breakthrough data from cotransport experiments with kaolinite particles and NPs have six degrees of freedom, the developed cotransport model successfully matches the BTCs by tuning two constants only. This validates the developed model for cotransport of two colloidal populations with different attachments and straining rates.

Keywords Colloidal transport · Nanoparticles · Cotransport · Analytical model · Attachment and straining

List of Symbols

- c Suspended concentration [ML^{-3}]
- C Normalised suspended concentration [–]
- k Permeability [L^2]
- S Retained concentration [ML^{-3}]

✉ P. Bedrikovetsky
pavel.russia@gmail.com

¹ Australian School of Petroleum, University of Adelaide, Adelaide, Australia

² School of Environmental Engineering, Technical University of Crete, Chania, Greece

s_m	Maximum attached concentration [ML^{-3}]
S	Normalised retained concentration [-]
t	Time [T]
T	Dimensionless time [PVI]
U	Flow velocity [LT^{-1}]
x	Axial coordinate [L]
X	Dimensionless axial coordinate [-]

Greek Letters

ϕ	Porosity [-]
λ_0	Initial attachment filtration coefficient [L^{-1}]
Λ_0	Dimensionless initial filtration coefficient [-]
λ_1	Size exclusion (straining) filtration coefficient [L^{-1}]
Λ_1	Dimensionless size exclusion filtration coefficient [-]
λ	Filtration coefficient [L^2M^{-1}]
μ	Viscosity [$\text{ML}^{-1}\text{T}^{-1}$]

Subscripts

K	Kaolinite
m	Maximum value
N	Nanoparticle

1 Introduction

Migration of suspended colloids predominately occurs in subsurface formations. However, flow of suspended colloids in porous media has also been observed in various processes of environmental, chemical, civil, and petroleum engineering (Civan 2015). Kaolinite clay particles are often present in numerous occasions of subterranean water contamination, plant irrigation, cold water injection into geothermal reservoirs, artificial recharge of aquifers, well drilling with filtrate invasion into formations, seawater intrusion into coastal aquifers, and low-salinity water injection into oilfields (You et al. 2015; Farajzadeh et al. 2017; Mirabolghasemi et al. 2015; Mikhailov et al. 2018). Kaolinite fines are detached from surfaces of sandstone rocks, yielding water contamination and permeability decline (Russell et al. 2017; Chequer et al. 2017).

Engineered nanoparticles have received considerable attention in a very large number of applications including the treatment of contaminated aquifers, fixing movable fines in oil and gas reservoirs for formation damage prevention (Arab et al. 2014; Yuan et al. 2016a; Yuan and Moghanloo 2017; Mansouri et al. 2019), and enhanced oil recovery by water flooding (Arab and Pourafshary 2013). The transport of NPs in porous media is relatively complicated, because it is affected by several factors including: interstitial velocity, solution chemistry, temperature, and the presence of other suspended particles (Rottman et al. 2013; Syngouna et al. 2017; Yuan et al. 2016b).

Numerous stochastic and deterministic mathematical models are developed to describe particle transport, capture, and the consequent rock alteration (Arab et al. 2014; Mirabolghasemi et al. 2015; Hammadi et al. 2017; Bashtani et al. 2018). The reviews by Shapiro and Yuan (2012) and Yuan et al. (2012) give a reasonably complete account of the available stochastic models. The stochastic models are described

by population balance equations (Sharma and Yortsos 1987; Santos and Bedrikovetsky 2006; Bedrikovetsky et al. 2017; Hayek et al. 2012), random walk models (Shapiro and Bedrikovetsky 2008, 2010; Yuan et al. 2012), deep bed filtration equation with stochastically distributed filtration coefficient (Yuan and Shapiro 2010; Elimelech et al. 2013), and Boltzmann's equation (Shapiro and Wesselingh 2008). Shapiro et al. 2007 derived deep bed filtration equations with incomplete pore plugging and derived exact solutions for 1D flows.

Averaging (aggregation and upscaling) of stochastic models with size-distributed particles and pores and multiple capture mechanisms is necessary to reduce the numerical burden. Guedes et al. (2009) proposed the mathematical procedure allowing aggregating multiple kinetic rate equations for particle retention into a single equation for the capture rate for dispersion-free transport. This method has been recently extended for advective-capture flow with dispersion (Zhang et al. 2018). Population balance equations with probabilistic distribution of pore and particle sizes allow for exact upscaling for suspensions of uniform size, and the resulting system coincides with the classical filtration equations for the averaged values (Bedrikovetsky 2008).

Several mathematical models for deep bed filtration of individual (transport) as well as binary mixtures (cotransport) are available in the literature (Abdel-Salam and Chrysikopoulos 1995; Bekhit et al. 2009; Katzourakis and Chrysikopoulos 2014, 2015). The common assumption is proportionality between the particle capture rate and the advective particle flux; their ratio is called the filtration function. The nonlinear deterministic deep bed filtration model allows for an exact solution (Polyanin and Manzhurov 2006; Polyanin and Zaitsev 2012). Furthermore, exact solutions for direct problem yield regularisation of the corresponding inverse problems, which allow for determination of the associated model functions from the laboratory tests (Alvarez et al. 2005, 2007; Hayek 2015; Hayek et al. 2012). An analytical model for deep bed filtration of a binary mixture, where each species is captured by a separate capture mechanism, using constant and Langmuir's filtration functions, is proposed in Araújo and Santos (2013). However, recent studies have shown that for kaolinite and graphene oxide (GO) NP cotransport, the attachment processes can be simultaneous for both suspended particles (Chrysikopoulos et al. 2017; Sotirelis and Chrysikopoulos 2017). Because suspended particles near rough pore walls migrate with significantly smaller velocity than the mean interstitial velocity (Sefrioui et al. 2013), several investigators proposed mathematical models for two populations of particles with two different velocities (Yuan and Shapiro 2010; Bradford et al. 2009b; Kuzmina et al. 2017). Yuan and Moghanloo (2017) and Yuan et al. (2016a) proposed mathematical models for kaolinite and NPs cotransport with adsorption as a major capture mechanism. However, a mathematical model for cotransport of colloids and NPs with simultaneous attachment and straining (size exclusion) of both species is not available.

The objective of the present work is to develop a mathematical model for cotransport of colloids and NPs in porous media using a novel filtration function capable of matching closely the experimental data collected by Chrysikopoulos et al. (2017) for kaolinite and NPs transport. The proposed novel filtration function incorporates two simultaneous capture mechanisms: Langmuir (blocking) and constant (low-retention) filtration. The cotransport model successfully matches six-dimensional set of the laboratory data on commingled injection of kaolinite and nanoparticles by tuning two model coefficients only, which validates the model.

2 Theoretical Developments

This section proposes the so-called binary filtration function that yields the BTCs with stabilised concentration lower than the injected concentration (Sect. 2.1), derives the exact solution for 1D transport of single colloidal population (Sect. 2.2, Table 1) and performs its qualitative analysis (Sect. 2.3). Then, we extend the binary filtration function for two-population transport, and develop the cotransport equations (Sect. 2.4), which are solved numerically (Sect. 2.5).

2.1 Transport Models for a Single-Particle Population

Assuming that the interstitial fluid is incompressible (water), the suspended particles are uniformly sized, particle concentration is low so that the carrier fluid density is not altered, particle dispersion (diffusion) is negligible compared to the interstitial velocity, particle capture by the solid matrix follows linear kinetics with capture rate proportional to the particle advective flux and occurs by size exclusion, straining, attachment, segregation, diffusion into dead-end pores, etc. (see Fig. 1a), permeability decline due to particle retention is adequately described Darcy's law, and the governing equations for transport in porous media are as follows (Herzig et al. 1970; Alvarez et al. 2005, 2007):

$$\frac{\partial}{\partial t}(\phi c + s) + U \frac{\partial c}{\partial x} = 0, \quad (1)$$

$$\frac{\partial s}{\partial t} = \lambda(s)cU, \quad (2)$$

$$U = -\frac{k(s)}{\mu(c)} \frac{\partial P}{\partial x}, \quad (3)$$

where x is the linear coordinate in the flow direction, t is time, c and s are the suspended and attached concentrations, ϕ is the porosity, U is the fluid velocity, λ is the filtration coefficient, k is the permeability, μ is the viscosity, and P is the pressure. The suspended particle concentration c is determined as the number of suspended particles in a unit volume of carrier fluid, while the retained particle concentration s is equal to the number of attached particles in a unit volume of the solid matrix. It should be noted that the effects of particle retention are in decreasing the suspended particle concentration and permeability. The suspended particle concentration decline due to retention is important for industrial waste disposal and aquifer contamination, while the permeability decline yields the impairment of production and injection wells.

For constant particle concentration injection in a typical bench-scale core or packed column, initially free of particles, the appropriate initial and boundary conditions are (Fig. 2):

$$c(x, 0) = s(x, 0) = 0, \quad (4)$$

$$c(0, t) = c^0, \quad (5)$$

where c^0 is the injected suspended particle concentration. The assumptions of a monolayer particle attachment (Langmuir type), where one attached particle occupies one vacancy,

Table 1 Explicit dimensionless expressions for suspended and attached particle concentrations

Zone	Domains	$C(X, T)$	$S(X, T)$
0	$T(X) \leq X$	0	0
I	$X < T(X) \leq X + T_m$	$\frac{1}{\left[1 - \exp\left[-\frac{\Delta_0}{S_m}(T-X)\right] + \exp\left[(A_0+A_1)X - \frac{\Delta_0}{S_m}(T-X)\right]\right]}$	$\frac{S_m}{\left[1 - \exp\left[-\frac{\Delta_0}{S_m}(T-X)\right] + \exp\left[(A_0+A_1)X - \frac{\Delta_0}{S_m}(T-X)\right]\right]}$
II	$X + T_m < T(X) < \frac{S_m}{A_1}(\exp(A_1X) - 1) + X + T_m$	$\frac{S_m}{\left[A_1(T-X - T_{cr}) + S_m\right] \left\{ \frac{A_1}{A_0} \exp\left[(A_0+A_1)X - \frac{1}{A_1} \ln\left[\frac{\Delta_1}{S_m}(T-X - T_{cr}) + 1\right]\right] + 1 \right\}}$	$\frac{S_m}{\left[A_1(T-X - T_m) + S_m\right] \exp\left[-\frac{\Delta_0 \Delta_1}{A_0}\right]}$
III	$T(X) \geq \frac{S_m}{A_1}(\exp(A_1X) - 1) + X + T_m$	$\exp(-A_1X)$	$\left[A_1(T-X - T_m) + S_m\right] \exp(-A_1X)$

Fig. 1 Multiple particle capture mechanisms: **a** various capture mechanisms at the pore scale; **b** attachment and straining of nanoparticles and clay particles

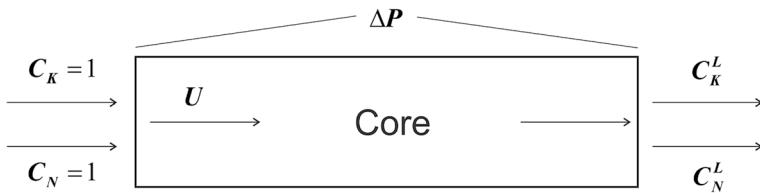
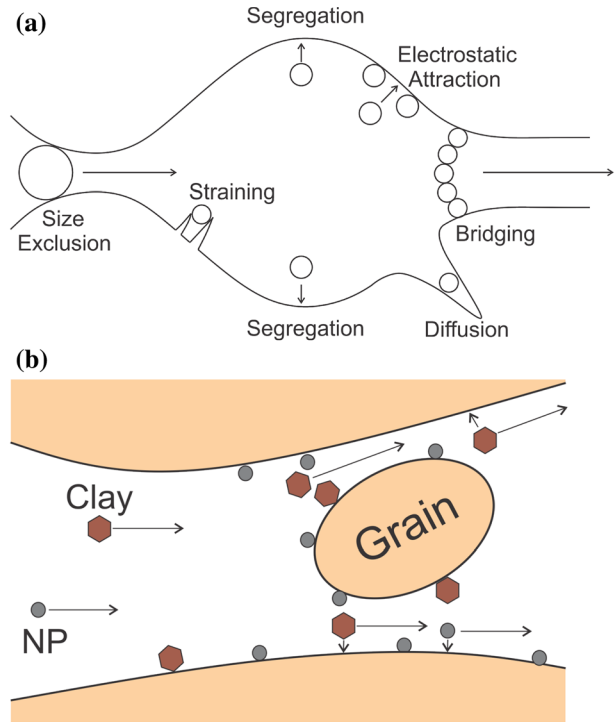


Fig. 2 Schematic illustration of a bench-scale porous medium. Kaolinite clay particles (C_K) and nanoparticles (C_N) are injected simultaneously. The dimensionless inlet concentrations are equal to one ($C_K = C_N = 1$)

and of the small suspended and attached particle concentrations, yield the following “active-mass” law for the particle–vacancy “reaction” (Elimelech et al. 2013).

$$\lambda(s) = \begin{cases} \lambda_0 \left(1 - \frac{s}{s_m}\right), & s < s_m \\ 0, & s > s_m \end{cases}, \quad (6)$$

where λ_0 is the initial filtration coefficient as determined by the solid matrix–particle attraction and s_m is the maximum concentration of attached particles (Bedrikovetsky 2008). Langmuir’s filtration function is given by curve 2 in Fig. 3b. The maximum value s_m corresponds to complete occupation of the solid matrix surfaces by the attached particles, and $1/s_m$ relates to the solid matrix fraction occupied by a single particle. After the retained

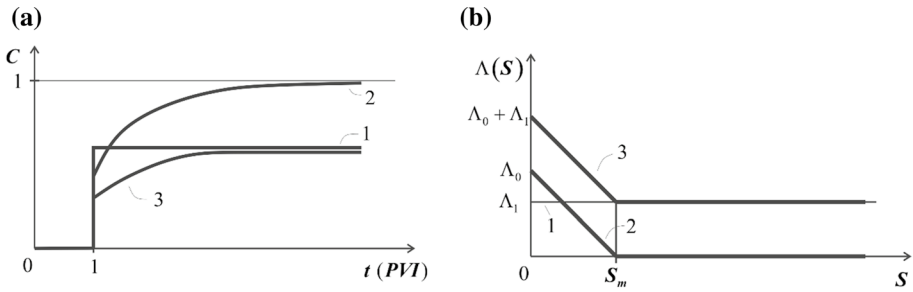


Fig. 3 Illustration of three different shapes of filtration function: **a** breakthrough curves (BTCs) and **b** shapes of filtration function. Curves 1, 2, and 3 correspond to constant filtration coefficient, Langmuir blocking, and combined (binary) filtration function for two simultaneous mechanisms, respectively

particle concentration reached its maximum value s_m , the particle attachment on the solid matrix surfaces stops. Note that the above-mentioned scenario corresponds to the case of solid matrix–particle attraction and particle–particle repulsion (Kuhnen et al. 2000; Ben-nacer et al. 2017). The Langmuir blocking filtration function (6) is usually used for monolayer electrostatic attachment of particles on solid matrix surfaces, but is also applicable for straining and size exclusion (Herzig et al. 1970; Kuhnen et al. 2000).

For a small retained particle concentration ($s \ll s_m$), the filtration coefficient is assumed to be constant, $\lambda(s) = \lambda_1$ (curve 1 in Fig. 3b). The probability of particle capture remains constant for low-retention concentrations, because the particles do not compete for the same vacancy. For this case, the breakthrough concentration is expected to be initially equal to zero and subsequently to jump up to some value that remains constant (curve 1 in Fig. 3a). In the present work, to be specific but without loss of generality, this low-retention mechanism is referred to as size exclusion, whereas attachment corresponds to the Langmuir’s blocking capture.

Regarding deep bed filtration with multiple particle capture mechanisms, Appendix A proves that the total retention rate for a multiple capture system can be represented by a single-capture mechanism given by Eq. (2). The overall filtration function $\lambda(s)$ is a total of individual filtration functions ($\lambda_1, \lambda_2, \dots, \lambda_n$), i.e. λ is also a function of all individual retention concentrations $s_i, i = 1, 2, \dots, n$. However, solution of system of retention rate Eq. (A1), where time T is parametrised by the total retention concentration $s(x_0, t)$, allows expressing all individual retention concentrations via the overall s , yielding the aggregated filtration function $\lambda = \lambda(s)$.

In particular, the filtration function that aggregates two capture mechanisms with Langmuir’s and constant filtration functions can be approximated by the following piecewise function with high accuracy (Zhang et al. 2018):

$$\lambda(s) = \begin{cases} \lambda_0 \left(1 - \frac{s}{s_m}\right) + \lambda_1, & s \leq s_m \\ \lambda_1, & s > s_m \end{cases}, \tag{7}$$

where the filtration coefficient λ_0 corresponds to monolayer attachment where no particles were attached yet, and λ_1 corresponds to low-retention size exclusion. So, the filtration function given by Eq. (7) consists of two simultaneous particle capture mechanisms and is called the binary filtration function further in the text. Curve 3 in Fig. 3b corresponds to

a binary filtration function. It should be noted that the filtration model (7) contains three parameters (λ_0 , λ_1 , and s_m). Model (7) can describe other couples of particle retention mechanisms.

Note that BTCs, which are initially equal to zero, jump up to some value and then monotonically increase to a limit that is lower than the injected concentration as time tends to infinity, have been observed in laboratory breakthrough experiments with kaolinite colloid particles and graphene oxide nanoparticles conducted by Chrysikopoulos et al. (2017).

In this study, we show that such BTCs can be represented by a binary filtration function.

Further in this paper, the filtration coefficients are determined by tuning the experimental data (Sect. 3). Theoretical calculations of straining filtration coefficient accounting for effects of attached particles can be performed from reconstruction of CT or NMR images using digital core techniques (Wang et al. 2018a, b; Shikhov and Arns 2015). The approach is similar to calculation of permeability or electrical conductivity from rock geometry at pore scale (Yanici et al. 2013; Arns and Adler 2018).

Introducing the following dimensionless definitions for time, x -coordinate, filtration coefficients, suspended and attached concentrations:

$$T = \frac{Ut}{\phi L}, X = \frac{x}{L}, A_i = \lambda_i L, C = \frac{c}{c^0}, S = \frac{s}{\phi c^0}, \quad (8)$$

the governing model (1, 2) becomes:

$$\frac{\partial(C+S)}{\partial T} + \frac{\partial C}{\partial X} = 0, \quad (9)$$

$$\frac{\partial S}{\partial T} = \Lambda(S)C, \quad (10)$$

Here, the filtration function (7) is given by:

$$\Lambda(S) = \begin{cases} \Lambda_0 \left(1 - \frac{S}{s_m}\right) + \Lambda_1, & S \leq S_m \\ \Lambda_1, & S \leq S_m \end{cases}, \quad (11)$$

and the initial and boundary conditions (4, 5) become:

$$C(X, 0) = S(X, 0) = 0, \quad (12)$$

$$C(0, T) = 1. \quad (13)$$

2.2 Analytical Model for 1D Flow of Single-Population Colloids

In this section, we present the final formulae for the analytical model for 1D flow of single-population colloids, derived in Appendix A. The formulation of the problem (9–13) corresponds to injection of particles with given suspended concentration into a porous specimen (Fig. 2).

Briefly, introducing the following integral potential from Eq. (10)

$$\Psi(S) = \int_0^S \frac{dy}{\Lambda(y)} \quad (14)$$

yields the following solution:

$$\int_{S(0,T-X)}^{S(X,T)} \frac{dS}{S\Lambda(S)} = -X, \quad \Psi(S(0, T - X)) = T - X, \quad T > X. \tag{15}$$

Equation (15) is the solution for retained particle concentration $S(X, T)$ at $T > X$. The solution for suspension concentration $C(X, T)$ follows from Eq. (B8) and boundary condition (13):

$$C(X, T) = \frac{S(X, T)}{S(0, T - X)}, \quad T > X. \tag{16}$$

The concentration front $X=T$ moves along the porous medium with a velocity equal to unity. Ahead of this front, initial conditions (12) hold: $C(X, T)=S(X, T)=0$. Along the front, the concentration of deposited particles equals zero, $S(T, T)=0$. Therefore, as it follows from Eqs. (9, 10), the concentration of suspended particles along the front, $C(T, T)$, is expressed as:

$$C(T, T) = \exp(-\Lambda(0)T). \tag{17}$$

Equations (15, 16) determine the retained particle concentration $S(X, T)$ for $T > X$. For $T < X$, integration along the characteristics of Eq. (A4) gives: $S(X, T)=0$. Substitution of Eq. (10) into Eq. (9) and integration along its characteristics for $T < X$ gives: $C(X, T)=0$.

Equation (15) provides an exact solution in the implicit form of two transcendental equations for unknowns $S(X, T)$ and $S(0, T)$. Using $S(0, T)$ as an independent variable allows for explicit calculation of T . The explicit formulae for suspended and retained particle concentrations are given in Table 1 for a binary filtration function.

2.3 Qualitative Analysis of the Flux Structure and Type Curves

Figure 3a presents three breakthrough curves simulated by the analytical solutions given in Table 1, for the three different filtration functions presented in Fig. 3b. The analytical solutions for the case of constant filtration coefficient are obtained by fixing $\Lambda_0=0$ and $S_m \rightarrow \infty$, and for Langmuir blocking function by setting $\Lambda_1=0$. The BTC corresponding to the constant filtration function is shown in Fig. 3a (curve 1), to the Langmuir filtration function is shown in Fig. 3a (curve 2), and to the case of combined constant and Langmuir filtration is shown in Fig. 3a (curve 3). The Langmuir mechanism exhibits blocking under conditions of substantial particle attachment. The Langmuir mechanism is usually applied for monolayer particle attachment onto the solid matrix, where the attachment rate is proportional to number of vacant sites for retention on the surfaces of solid matrix.

Figure 4a shows the plane (X, T) , three concentration fronts, and the corresponding flow zones: 0, I, II, and III, as obtained by the exact analytical solutions listed in Table 1. The four different zones are separated by the trajectories of three concentration fronts: $T_I(X)$, $T_{II}(X)$, and $T_{III}(X)$. The corresponding domains separated by those fronts are presented in Table 1. The cotangents of the trajectory slopes $(dT_k(X)/dX)^{-1}$, $k=I, II, III$, are equal to the front speeds. Note that the method of characteristics was used for the derivation of the exact solutions presented in Table 1, and the characteristics are the particle trajectories. The initial conditions hold in zone 0 ahead of the concentration front $T_I(X)$ that moves

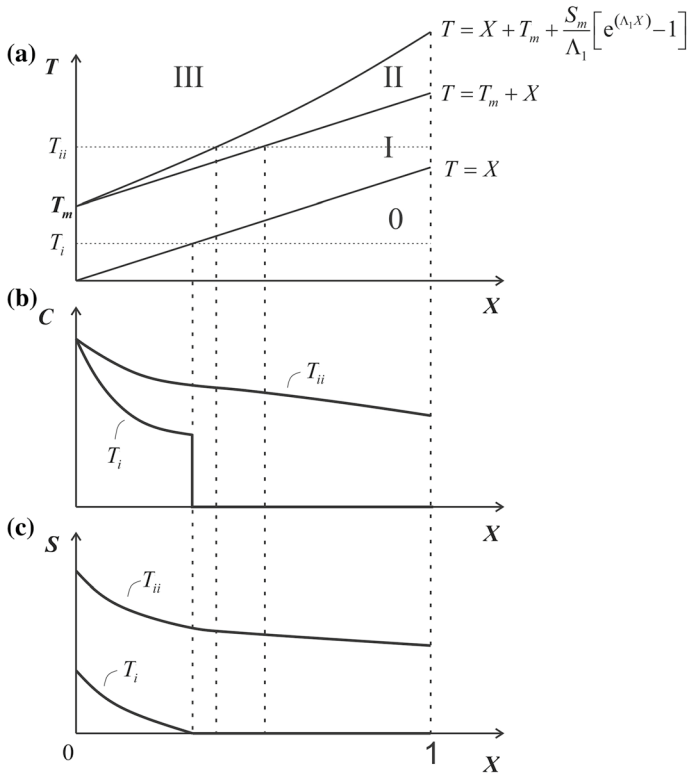


Fig. 4 Exact solution for particle transport in porous media with piecewise-linear filtration function: **a** structure of the flow pattern, **b** suspended particle concentration profiles at three instances, and **c** retained particle concentration profiles at three instances

with unitary speed. Zone I behind this front corresponds to flow with retained concentration $S(X, T) < S_m$, where the particles migrate subject to binary filtration function (7). Two capture mechanisms act in zone I. The filtration function is constant in zone III, where the suspended particles move from the inlet $X=0$ to the boundary between zones III and II, $T_{III}(X)$, where the retained particle concentration increases up to the maximum value S_m . Migration of suspended particles continues in zone II subject to linear filtration. Only straining occurs in zone III, while both retaining mechanisms act in zone II. The suspended particle concentration is at a steady state in zone III, so the capture rate is constant, and the retained particle concentration accumulates linearly with time. The structure of the flow pattern is as follows: (Zone 0)—initial conditions of no suspended and retained particles are held ahead of the first concentration front; (Zone I)—two simultaneous capture mechanisms act, front and rear boundaries of this zone move with unitary speed; (Zone II)—starts at the inlet at the moment T_m , when the maximum attached value S_m is reached by the retained particle concentration; subsequently, only straining occurs in zone III; and (Zone III)—steady-state suspended particle concentration decreases exponentially due to constant filtration. Figure 4b, c present profiles of suspended and retained particles at three different points in time. At T_i , the particle front did not breakthrough yet. Both dimensionless particle concentrations C and S are zero ahead of this front. The suspended particle

concentration jumps from zero at the front and increases behind the front, while the suspended particle concentration is continuous. At T_{ii} , after the front has breakthrough, the profiles of particle concentration decrease exponentially from the inlet in zone III, and continue to decrease in zones II and I. Suspended particle concentrations coincide at T_{ii} and T_{iii} in zone III.

2.4 Cotransport Model

For the case of cotransport of two different populations of suspended particles, it was assumed that the concentration of each population of suspended particles was low, so that the suspended particles from one population do not compete for the same vacancies with suspended particles from the other population (Fig. 1b). The particle capture by the solid matrix for each population follows linear kinetics with capture rate proportional to the particle advective flux and occurs by either two mechanisms of size exclusion, straining, attachment, segregation, diffusion into dead-end pores, etc. (see Fig. 1a). Therefore, the maximum attached particle concentration S_m and attachment filtration coefficient Λ_0 of each population during cotransport are assumed to be identical to those during transport of each individual population. The suspended particles of each population are uniformly sized and, being attached, occupy the same surface area. The interstitial carrier fluid is incompressible. Particle concentration in each population is low, so that the carrier fluid density is not altered. Consequently, for the case of kaolinite colloids and NPs cotransport the governing partial differential equations are (Bedrikovetsky 2013):

$$\frac{\partial C_i}{\partial T} + \frac{\partial C_i}{\partial X} = - \left[\Lambda_{0i} \left(1 - \frac{S_N}{S_{mN}} - \frac{S_K}{S_{mK}} \right) + \Lambda_{1i} \right] C_i, \quad (18)$$

$$\frac{\partial S_i}{\partial T} = \left[\Lambda_{0i} \left(1 - \frac{S_K}{S_{mK}} - \frac{S_N}{S_{mN}} \right) + \Lambda_{1i} \right] C_i \quad (19)$$

where index $i=K, N$ corresponds to kaolinite colloids and NPs, respectively. It should be noted that S_{mN} , Λ_{0N} , S_{mK} , and Λ_{0K} are equal to those for the case of transport of each population of suspended particles, but Λ_{1N} and Λ_{1K} are different because particle onto the surfaces of the solid matrix can affect pore throat radii (Fig. 1b), which in turn can affect straining (Fig. 1b) (Alem et al. 2015). Therefore, the filtration coefficients for straining during cotransport are assumed to be different from those corresponding to transport of each individual population. The cotransport model contains six independent parameters: S_{mN} , Λ_{0N} , S_{mK} , Λ_{0K} , Λ_{1N} and Λ_{1K} . Four parameters (S_{mN} , Λ_{0N} , S_{mK} , and Λ_{0K}) are determined from experimental breakthrough data of individual population transport, whereas two parameters (Λ_{1N} and Λ_{1K}) are obtained by fitting the cotransport experimental breakthrough curves.

The initial and boundary conditions for system (18, 19) corresponding to commingled injection of kaolinite and NPs are

$$C_K(X, 0) = C_N(X, 0) = S_K(X, 0) = S_N(X, 0) = 0, \quad (20)$$

$$C_K(0, T) = C_N(0, T) = 1. \quad (21)$$

2.5 Numerical Modelling of Single and Binary Suspension-Colloidal Populations

The governing equations subject to initial and boundary conditions for individual transport (9–13) and for cotransport (18–21) were solved numerically using the computer code developed by Shampine (2005a). The inbuilt algorithm implements a two-step Lax–Friedrichs finite-difference method (Shampine 2005b). The method allows for vectorisation of the problem, taking advantage of MATLAB’s matrices and vectors optimisation. The MATLAB computer program and pertinent supporting information are available from <http://faculty.smu.edu/shampine/current.html>. We divide the spatial domain $[0,1]$ into 1000 evenly spaced intervals, so $\Delta X=0.001$. The time steps employed in the finite-difference method is selected to satisfy the Courant–Friedrichs–Lewy stability condition, $\Delta T=0.0009$. Both species during the individual and binary flows move with the carrier water velocity (see Eqs. 9 and 18), so time step ΔT is taken the same for individual flow and for cotransport.

Figure 5 presents a comparison of the analytical solution with the numerical solution for individual transport of NPs and kaolinite colloids at $\text{pH}=7$ and $I_S=27$ mM. The values of the parameters Λ_0 , Λ_1 , and S_m used are listed in Table 2. The exact analytical and numerical solutions are almost identical. Smoothing of the concentration jump in the numerical solution is almost invisible, suggesting that the numerical scheme exhibited very low numerical dispersion.

Figures 8 and 9b present BTCs, calculated numerically for NPs and kaolinite fines during the cotransport.

3 Results

The new transport and cotransport mathematical models were used to match the experimental data reported by Chrysikopoulos et al. (2017) for transport and cotransport of graphene oxide (GO) NPs and kaolinite (KGa-1b) colloids in columns packed with glass beads and quartz sand under various water chemistry conditions ($\text{pH}=4, 7, 10$ and $I_S=7, 12, 27$ mM). The unknown parameters were determined with a nonlinear least squares method, which minimises the normalised deviation between the model and the experimental data (Coleman and Li 1996). Specifically, the Trust-Region-Reflective optimisation algorithm

Fig. 5 Comparison between the analytical and numerical modelling for individual suspended particle transport

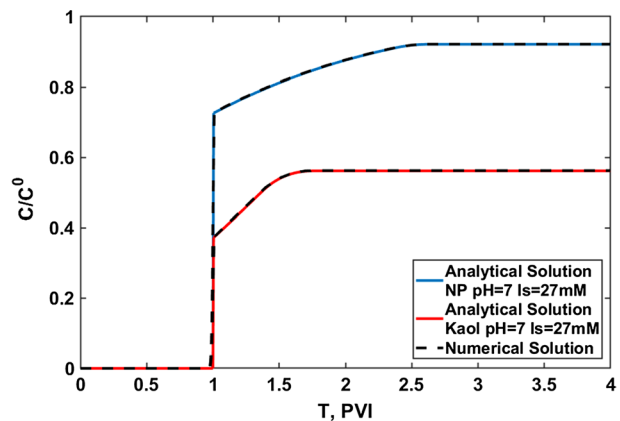


Table 2 Fitted parameters for GO NPs and kaolinite colloids individual transport experimental data

Figure	Glass beads									
	GO NPs					Kaolinite colloids				
	A_0	A_1	S_M	T_m	R^2	A_0	A_1	S_M	T_m	R^2
(a) pH=4 $I_S=7$ mM	0.4888	0.0910	0.5953	2.2555	0.9536	0.3506	0.5110	0.7629	1.1368	0.8815
(b) pH=7 $I_S=7$ mM	0.3045	0.0451	0.1216	0.8180	0.9598	0.2536	0.4395	0.3113	0.5592	0.9754
(c) pH=10 $I_S=7$ mM	0.1684	–	0.0731	–	0.9863	0.2211	0.4233	0.3898	0.7409	0.9751
(e) pH=7 $I_S=12$ mM	0.1956	0.0465	0.1233	1.0402	0.9851	0.6283	0.3526	0.3032	0.4938	0.9841
(f) pH=7 $I_S=27$ mM	0.2395	0.0821	0.2433	1.3870	0.9807	0.4130	0.5813	0.2847	0.3700	0.9276
pH=7 $I_S=7$ mM	Sand									
	Nanoparticles					Kaolinite				
	A_0	A_1	S_M	T_m	R^2	A_0	A_1	S_M	T_m	R^2
	0.9279	0.0529	0.2542	0.7998	0.9396	0.7186	0.1371	0.2542	0.6478	0.9597

of MATLAB was used for the solution of the resulting quadratic-deviation minimisation problem. Note that the steep continuous growth of a BTC around its breakthrough time ($T=1$) is treated in this work as a concentration jump from zero, before the breakthrough to continuously growing BTC after the breakthrough. The areas between the continuous and discontinuous BTCs before and after the breakthrough time are equal. This procedure used here for matching BTCs is analogous to matching of inner and outer asymptotic expansions when dispersion is small (Polyanin and Dil'man 1994; Polyanin 2004).

3.1 Matching of the Transport Experimental Data

The experimental data for NPs and for kaolinite colloids individual transport in a column packed with glass beads at five different sets of water chemistry conditions reported by Chrysikopoulos et al. (2017) are presented in Fig. 6, together with the corresponding fitted analytical model simulations. Furthermore, the experimental data for NPs and for kaolinite colloids individual transport in a column packed with quartz sand for just one set of water chemistry conditions are presented in Fig. 9a, together with the corresponding fitted analytical model simulations. All fitted parameters for the individual transport experiments are listed in Table 2. Based on the R^2 values listed in Table 2, the analytical model fitted adequately the experimental data for both NPs and kaolinite colloids. This validates the proposed binary model given by Eq. (7).

For all cases presented in Fig. 6 (except the NP case in Fig. 6c), the experimental data were fitted with the analytical model utilising the filtration piecewise function (7). The unfavourable attachment conditions (high pH and low I_S) in Fig. 6c lead to large

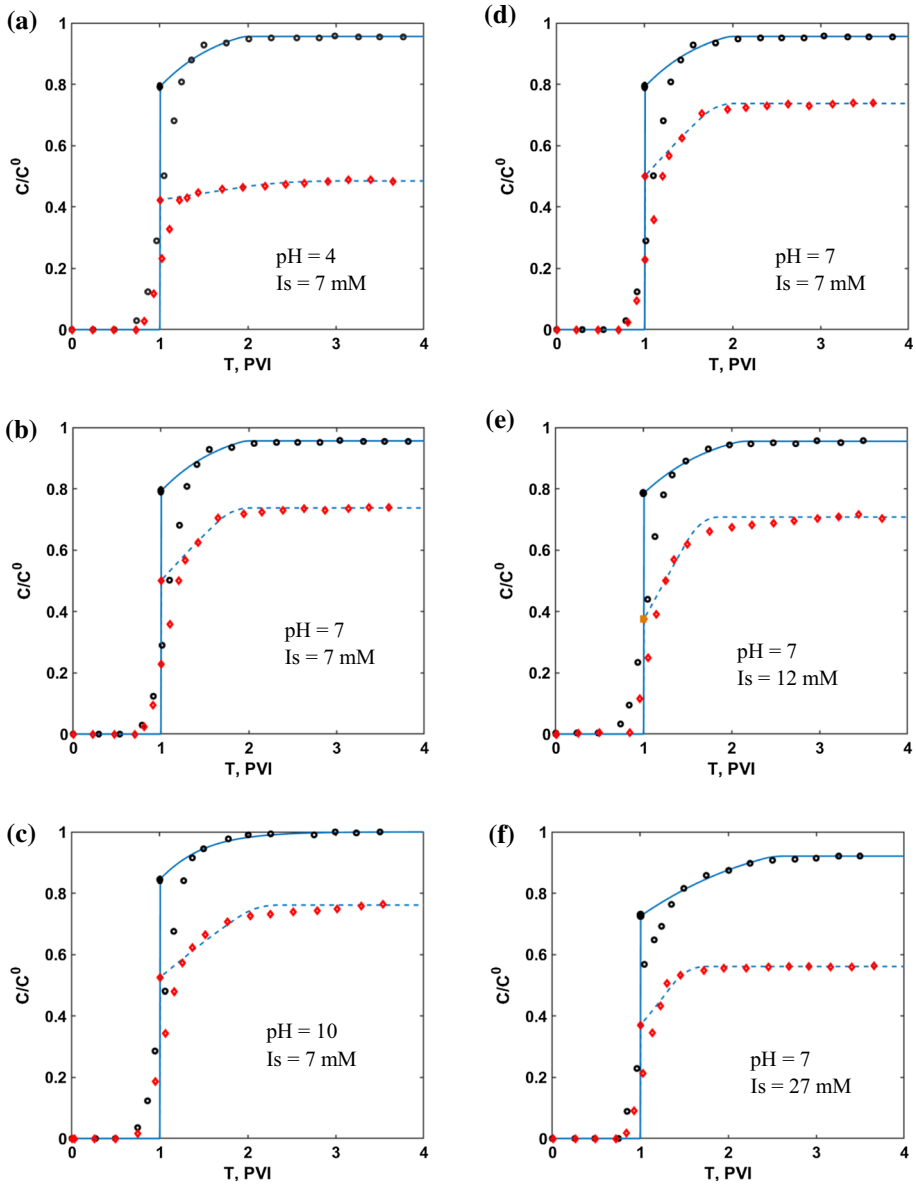


Fig. 6 Fitted breakthrough data reported by Chrysikopoulos et al. (2017) for individual transport experiments of GO NPs (open black circles) and kaolinite colloids (red diamonds) in columns packed with glass beads at different conditions: **a** pH=4, $I_s=7$ mM, **b** and **d** pH=7, $I_s=7$ mM, **c** pH=10, $I_s=7$ mM, **e** pH=7, $I_s=12$ mM, and **f** pH=7, $I_s=27$ mM. BTC tending to unity is fitted with a Langmuir function (solid curves in **c**), while those tending to the limit below unity are fitted with a piecewise filtration function

solid matrix–particle repulsion, as suggested by (Derjaguin–Landau–Verwey–Overbeek) DLVO theory (Chrysikopoulos et al. 2017). Consequently, suspended particles are mobile and unstable (Bennacer et al. 2017). Furthermore, attachment onto the solid matrix under

unfavourable attachment conditions can be better represented by the Langmuir filtration function.

The fitted parameters listed in Table 2 are also presented graphically in Fig. 7 as a function of pH and I_s . Parameter values, corresponding to transport experiments in columns packed with glass beads and quartz sand, are represented by circles and squares, respectively. Figures 7a and 4d show the initial filtration coefficient variability with pH, at $I_s=7$ mM for NPs and kaolinite colloids, respectively. The higher is the pH, the lower is the electrostatic solid matrix–particle attraction, and the lower is the Λ_0 as well as the straining Λ_1 (Bradford et al. 2009a). Figures 7b and 7e show the initial filtration coefficient variability with I_s , at pH=7 for NPs and kaolinite colloids, respectively. The higher is the I_s , the larger is the expected electrostatic attraction between the suspended particles and the solid matrix, and in turn the higher the expected value for both filtration coefficients (Λ_0 and Λ_1). The Λ_0 fitted values for both NPs and kaolinite colloids do not exhibit a clear increasing trend with increasing I_s . However, the fitted values for Λ_1 for both NPs and

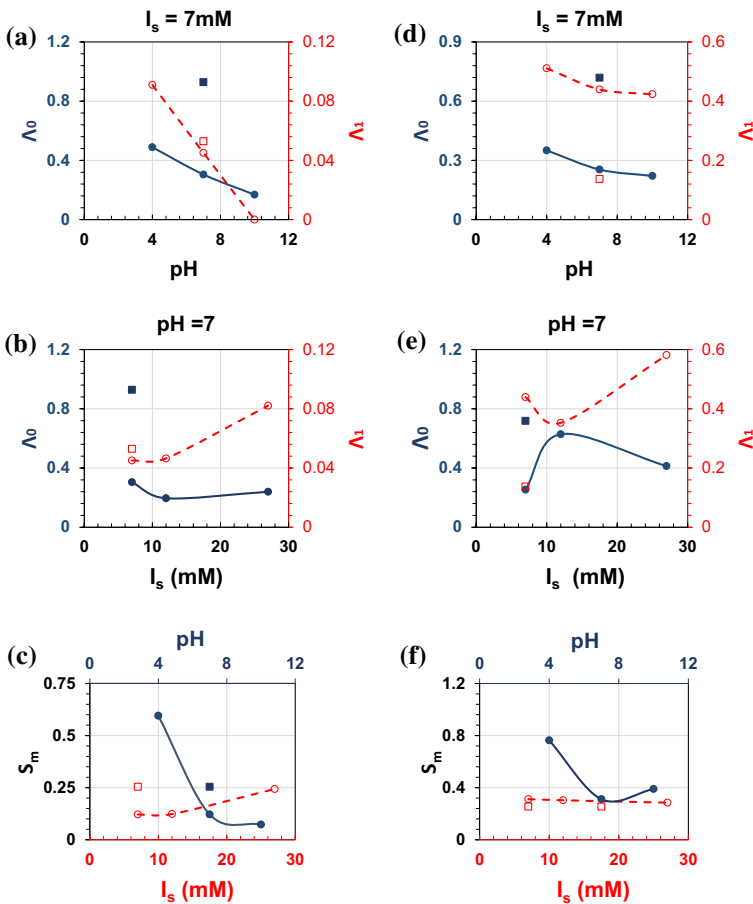


Fig. 7 Behaviour of fitted parameters for individual transport experiments of: **a–c** GO NPs and **d–e** kaolinite colloids as a function of pH and I_s . Circles and squares correspond to columns packed with glass beads and quartz sand, respectively. Solid and open symbols in **a, b, d, e** correspond to parameters Λ_0 and Λ_1 , respectively. Solid and open symbols in **c, f** correspond to parameter variation with pH and I_s , respectively

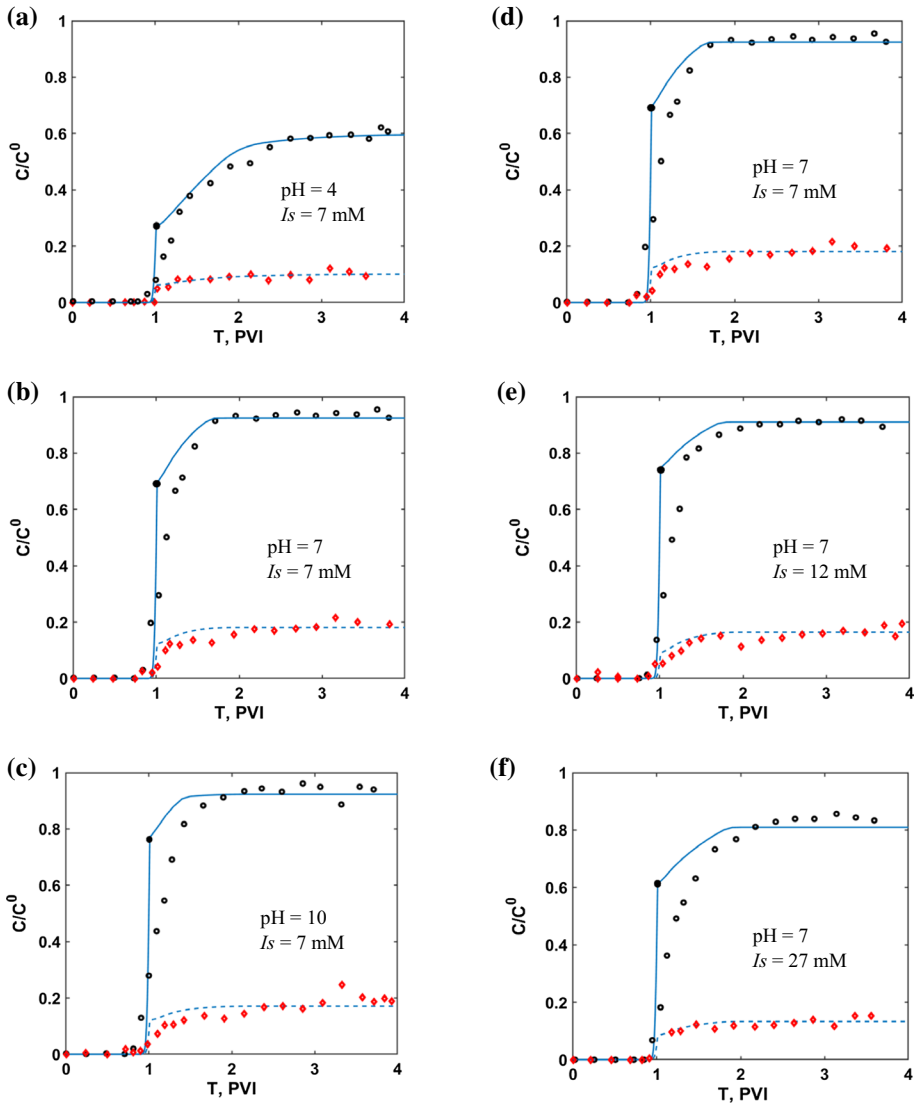


Fig. 8 Fitted breakthrough data reported by Chrysikopoulos et al. (2017) for cotransport experiments of GO NPs (open black circles) and kaolinite colloids (red diamonds) in columns packed with glass beads at different conditions: **a** pH = 4, $I_S = 7$ mM, **b** and **d** pH = 7, $I_S = 7$ mM, **c** pH = 10, $I_S = 7$ mM, **e** pH = 7, $I_S = 12$ mM, and **f** pH = 7, $I_S = 27$ mM. The matched modelling data are given by continuous curves

kaolinite colloids generally fulfil this tendency. Figure 7c and f shows the maximum retention concentration variability with I_S and pH for both NPs and kaolinite colloids, respectively. For increasing pH and decreasing I_S , both the electrostatic attraction between the suspended particles and the solid matrix and S_m are expected to decrease. This is clearly the case for NPs, but it is somewhat less pronounced for kaolinite colloids.

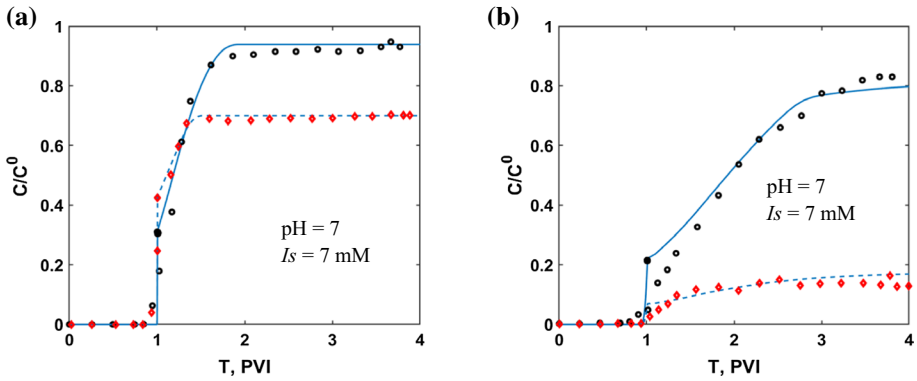


Fig. 9 Fitted breakthrough data reported by Chrysikopoulos et al. (2017) for **a** individual transport experiments of NPs (open black circles) and kaolinite colloids (red diamonds), and **b** cotransport experiments of GO NPs (open black circles) and kaolinite colloids (red diamonds) in columns packed with sand at pH=7 and $I_s=7$ mM. The matched modelling data are given by continuous curves

Table 3 Fitted parameters for GO NPs and kaolinite colloids cotransport experimental data

	Glass beads			
	GO NPs		Kaolinite colloids	
Figures 6, 7	$\Lambda_{1,N}$	R^2	$\Lambda_{1,K}$	R^2
(a) pH=4 $I_s=7$ mM	0.59	0.9142	2.32	0.9263
(b) pH=7 $I_s=7$ mM	0.22	0.9426	2.00	0.9296
(c) pH=10 $I_s=7$ mM	0.14	0.8925	1.95	0.8805
(e) pH=7 $I_s=12$ mM	0.21	0.9144	2.25	0.8968
(f) pH=7 $I_s=27$ mM	0.23	0.8770	2.20	0.8992
	Quartz sand			
	GO NPs		Kaolinite colloids	
Figure 8	$\Lambda_{N,coinj}$	R^2	$\Lambda_{k,coinj}$	R^2
pH=7 $I_s=7$ mM	1.00	0.9710	2.60	0.9381

The mean radius of the glass beads employed in this study was 1 mm, while the mean radius of quartz sand grain was 0.3 mm. So, the sand grains were smaller than the glass beads; thus, the solid matrix surface area was larger in the columns packed with quartz sand. Furthermore, sand grain shapes are irregular, so the surface area was larger than that

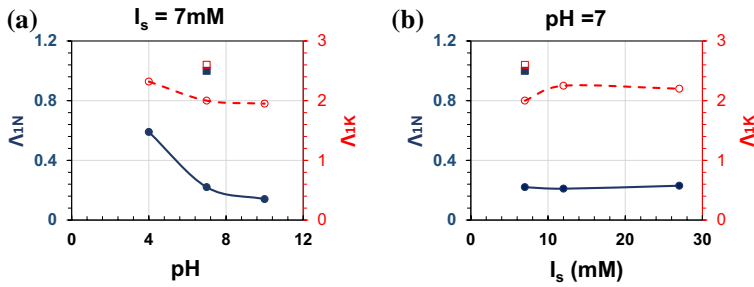


Fig. 10 Behaviour of fitted parameters associated with the cotransport experiments of GO NPs and kaolinite colloids as a function of: **a** pH and **b** IS. Circles and squares correspond to columns packed with glass beads and quartz sand, respectively. Solid and open symbols in **a**, **b** correspond to parameters Δ_{1N} (for GO NPs) and Δ_{1K} (for kaolinite), respectively

for the glass beads. Consequently, Λ_0 must be greater for quartz sand. This is clearly the case for both NPs and kaolinite colloids (see Fig. 7a, b, d, e) (Bradford et al. 2003, 2009a). The pore throats in columns packed with quartz sand are smaller than those packed with glass beads. Also, sand has rougher surface than glass beads, which facilitates size exclusion. The average radii for nanoparticles and kaolinite colloids were 0.4 μm and 0.6 μm , respectively, i.e. they are almost the same. Therefore, size exclusion filtration coefficient Λ_1 must be higher for sand than for glass beads. This is the case for NPs (see Fig. 7a, b), but not for kaolinite colloids (see Fig. 7d, e). The maximum retention concentration for columns packed with quartz sand is higher due to the larger solid matrix surface area of the smaller irregular grains. Therefore, S_m must be higher for columns packed with quartz. This is the case for NPs (see Fig. 7c), but not for kaolinite colloids (see Fig. 7f). The deviation of kaolinite colloids from expected behaviour is attributed to kaolinite particle aggregation. It should be noted that based on DLVO theory, kaolinite aggregation is significant (Chrysikopoulos et al. 2017).

3.2 Matching of the Cotransport Experimental Data

The experimental data for NPs and for kaolinite colloids cotransport in a column packed with glass beads at five different sets of water chemistry conditions reported by Chrysikopoulos et al. (2017) are presented in Fig. 8, together with the corresponding fitted numerical model simulations. Furthermore, the experimental data for NPs and for kaolinite colloids cotransport in a column packed with quartz sand for just one set of water chemistry conditions are presented in Fig. 9b, together with the corresponding fitted numerical model simulations. All fitted parameters for the cotransport experiments are listed in Table 3. Based on the R^2 values listed in Table 3, the numerical model (Eqs. 18 and 19) fitted adequately the experimental data for both NPs and kaolinite colloids. It should be noted that for individual suspended particle transport, the BTCs have an exponential form, so the number of degrees of freedom for each BTC is three. Therefore, three coefficients (Λ_0 , Λ_1 and S_m) are determined from experimental BTC. However, for the case of cotransport (Eqs. 18 and 19), there are two breakthrough curves with six degrees of freedom, and the number of fitted parameters is only two (Δ_{1N} and Δ_{1K}).

The fitted parameters listed in Table 3 are also presented graphically in Fig. 10 as a function of pH and I_S . Both Λ_{1N} and Λ_{1K} corresponding to NPs and kaolinite colloids, respectively, decrease with increasing pH, at $I_S = 7$ mM (see Fig. 10a), whereas both Λ_{1N} and Λ_{1K} , at pH = 7, are not strongly affected by I_S (see Fig. 10b). The unexpected behaviour of kaolinite colloids (Fig. 10b) is attributed to kaolinite–kaolinite particle aggregation, which is far more significant than that of kaolinite–NP and NP–NP (Chrysikopoulos et al. 2017). It should be noted that based on DLVO theory, kaolinite aggregation is significant (Chrysikopoulos et al. 2017). However, particle aggregation was beyond the scope of this study and has not been accounted for by the proposed transport and cotransport models.

4 Discussion

The fate and transport of nanoparticles and clays in subterranean waters are highly affected by the nanoparticle–clay interactions, cotransport and their capture by the porous matrix. In this study, a novel 1D transport model with binary filtration functions was developed to simulate the transport of suspended colloidal particles as well as the cotransport of colloids and NPs. The proposed cotransport model assumes that the different types of suspended particles have electrostatic interactions with the solid matrix, which are similar under both transport and cotransport conditions. Also, the initial attachment filtration coefficient for each particle type in the mixture is equal to that for transport of each individual particle type, which implies that the maximum retention concentration for attachment for each particle type is the same under both transport and cotransport conditions.

4.1 Validity of the Single-Population and Cotransport Models

The Langmuir's mechanism is usually applied for monolayer particle attachment to the rock, where the rate is proportional to number of vacant sites for retention on rock surface. However, for size exclusion in two-sized rock with mono-sized suspension transport, the filtration function also has the blocking form (Bedrikovetsky 2008).

The individual binary filtration function, given by Eq. (7), contains three constants, namely λ_0 , s_m , and λ_1 . The breakthrough curve, typical for individual corefloods by nanoparticles and kaolinite particles, has three degrees of freedom (Figs. 6, 7, 8). For 11 tests, the mathematical model for single-population deep bed filtration with binary function (7) closely matches the laboratory data. However, the degree of freedom of the matched numerical array does not exceed the number of the model constants, so the model validity cannot be claimed.

The cotransport model (18, 19) contains six constants, from which four constants are determined from the individual transport experimental data. This leaves just two tuning parameters λ_{1N} and λ_{1K} . Two BTCs for each component are closely matched, so the degree of freedom of the matched information array is six. High match between the laboratory and modelling data for six cotransport experiments performed allows validating the binary deep bed filtration model given by Eq. (18, 19). In particular, the assumption that the Langmuir coefficients for transport and cotransport of NPs and kaolinite colloids are the same is valid.

4.2 Effects of Rock Properties, Salinity, and pH

Comparison between columns packed by sand and by glass beads allows qualitative prediction for straining and attachment filtration coefficients, and also for maximum attached concentration S_m . The same relates to pH and salinity for water. Those dependencies are very clearly confirmed during corefloods by nanoparticles. However, the results for kaolinite injection do not follow the trend.

DLVO energy potentials show that the particle–particle attraction is significantly weaker than that for particle–rock (Sotirelis and Chrysikopoulos 2017; Chrysikopoulos et al. 2017). Besides, the attraction force kaolinite–kaolinite is significantly stronger than those for kaolinite–NP and NP–NP. Thus, aggregation of kaolinite–NP and NP–NP can be neglected, while the kaolinite–kaolinite aggregation must be accounted for in the basic model. The lack of aggregation for kaolinite in the model can be blamed for non-monotonic behaviour of the curves shown in Figs. 7 and 10. Therefore, the model for kaolinite should include aggregation, which is outside the scope of the present study and is the next stage of the work.

4.3 Front for Discontinuity of First Derivatives

First derivatives of the solution for piecewise-linear filtration function suffer discontinuity on the boundary between zones II and III, where $S(X, T) = S_m$, and the derivative of the filtration function is also discontinuous. This phenomenon has been observed from the exact solution for flow with deposit dissolution, where the dissolution rate becomes zero when the deposit vanishes (Sorbie and Stamatidou 2018). Apart from the derivative discontinuity front, the system with deposit dissolution is linear, and the complete dissolution front propagates with constant speed. The problem (9, 10) is nonlinear, so the front trajectory in Fig. 4a is curvilinear.

4.4 Application of the Model

The proposed cotransport model with two capture mechanisms can be also used for prediction of simultaneous flows of bacteria, viruses, clays, NPs, etc. Section 2.1 shows that the filtration coefficient is constant for small retained concentration under any capture mechanism (Fig. 3b). For intermediate retained concentrations, for any capture mechanism, keeping zero and first terms in the Taylor's series yields linear filtration function (6). Zhang et al. (2018) show that binary filtration function (7) is an approximation of any two simultaneous mechanisms with constant and linear filtration functions.

The exact solution for homogeneous colloid transport has been used to fit the laboratory data and obtain model coefficients. The matching process requires computing the direct (forward) model many times; and consequently, any incremental computation time introduced by numerical techniques can be prohibitive to convergence of the fitting procedure. Therefore, derived analytical model for binary particle capture mechanisms is preferred over computationally expensive numerical solutions of inverse problem for history matching. In addition, the exact solution presented here can be used as a benchmark for numerical models. The explicit analytical solution provided in Table 1 allows for direct numerical implementation without going through complicated mathematical derivations. The analytical model developed can also be used in three-dimensional reservoir simulation using stream-line techniques (Oladshkin and Panfilov 2007).

5 Conclusions

Analytical modelling of separate and commingled transport of clay particles and nanoparticles and matching the laboratory data allow drawing the following conclusions:

1. The breakthrough curves for *individual deep bed filtration* of kaolinite and nanoparticles exhibit the behaviour typical for two simultaneous particle capture mechanisms with binary filtration function. Tuning of six corefloods by kaolinite and six corefloods by nanoparticles and high agreement between the modelling and experimental data validate the two capture models for individual flows of both populations.
2. The proposed model for *commingled injection* of kaolinite and nanoparticles assumes the same electrostatic interaction between the species and the rock, as for the individual flows. Therefore, the initial attachment filtration coefficient for each species in the mixture is equal to that for the individual flow.
3. Another assumption of cotransport model is independent occupation of the attachment vacancies by both species, so the individual maximum retention concentration for attachment for each species is equal to that in the mixture.
4. The tuning parameters during matching the breakthrough curves with commingled injection are size exclusion filtration coefficients for straining, $\Lambda_{1,K}$, and $\Lambda_{1,N}$. High precision of the matching of eight-parametric experimental data array by two tuning parameters only for six commingled corefloods validates the cotransport model developed.

Appendix A: Aggregation of Multiple Particle Capture Mechanisms in One Mechanism

Following works by Guedes et al. (2009) and Zhang et al. (2018), in this Appendix we present the aggregation procedure for multiple particle capture mechanisms.

Consider single-population colloidal-suspension flow with n particle retention mechanisms that correspond to different filtration functions:

$$\frac{\partial S_i}{\partial T} = \Lambda_i(S_1, S_2 \dots S_n)C, \quad (\text{A1})$$

where the total retention concentration is a sum of individual retention concentrations

$$S = \sum_{i=1}^n S_i. \quad (\text{A2})$$

As it follows from Eq. (A2), mass balance for suspended particles and the particles retained by all capture mechanisms is given by Eq. (9).

The sum of n retention rates (A1) leads to the total retention rate of the overall colloidal suspension

$$\frac{\partial S}{\partial T} = \Lambda(S_1, S_2 \dots S_n)C, \quad \Lambda(S_1, S_2 \dots S_n) = \sum_{i=1}^n \Lambda_i(S_1, S_2 \dots S_n). \quad (\text{A3})$$

Here, $\Lambda(S_1, S_2, \dots, S_n)$ is the overall filtration function.

Fixing $x=x_0$, assuming that $C(X, T)$ is already known, and changing independent variable in system of ordinary differential equations (A3) from T to S yield

$$\frac{\partial S_i}{\partial S} = \frac{A_i(S_1, S_2 \dots S_n)}{\Lambda(S_1, S_2 \dots S_n)}, \quad \frac{\partial T}{\partial S} = \frac{1}{\Lambda(S_1, S_2 \dots S_n)}, \quad i = 1, 2 \dots n. \tag{A4}$$

Zero initial conditions for all retention concentrations yield initial condition (12) for the total retention concentration

$$S = 0 : S_i = 0, \quad i = 1, 2 \dots n. \tag{A5}$$

Substitution of solution of the problem (A4) $S_i=S_i(S)$ into Eq. (A5) yields

$$\frac{\partial S}{\partial T} = \Lambda(S_1(S), S_2(S) \dots S_n(S))C, \quad \Lambda(S) = \sum_{i=1}^n A_i(S_1(S), S_2(S) \dots S_n(S)), \tag{A6}$$

and reduces system of $n + 1$ Eqs. (9, A1) to two Eqs. (9, 10).

Appendix B. Exact Solution for 1D Transport of Single-Population Colloids

Following works by Polyanin and Manzhirov 2006; Polyanin and Zaitsev (2012); Alvarez et al. (2005, 2007); Bedrikovetsky et al. (2017), in this Appendix we derive an analytical solution to the model Eqs. (9–13).

Introduction of function $\Psi(S)$ by formula (14) yields the following form for Eq. (10):

$$\frac{\partial \Psi(S)}{\partial T} = C. \tag{B1}$$

Substituting expression (B1) for $C(X, T)$ into Eq. (9) and changing the order of differentiation by X and T in second derivative yield

$$\frac{\partial}{\partial T} \left[\frac{\partial \Psi(S)}{\partial T} \right] + \frac{\partial S}{\partial T} + \frac{\partial}{\partial T} \left[\frac{\partial \Psi(S)}{\partial X} \right] = 0. \tag{B2}$$

Integrating Eq. (B2) in T from 0 to T leads to the following expression:

$$\frac{\partial \Psi(S)}{\partial T} + S + \frac{\partial \Psi(S)}{\partial X} = \frac{\partial \Psi(S)}{\partial T} \Big|_{T=0} + S \Big|_{T=0} + \frac{\partial \Psi(S)}{\partial X} \Big|_{T=0}. \tag{B3}$$

The constant of integration is situated in the right-hand side of Eq. (B3) and is calculated from initial conditions (12). So, the right-hand side of the previous equation is equal to zero. Consequently, Eq. (B3) reduces to:

$$\frac{\partial \Psi(S)}{\partial T} + \frac{\partial \Psi(S)}{\partial X} = -S \tag{B4}$$

where $\Psi(X, T)$ is unknown, and $S(\Psi)$ is the inverse function to $\Psi=\Psi(S)$.

The initial and boundary conditions (12), (13) for Eq. (B4) become:

$$\Psi[S(X, 0)] = 0, \quad \Psi[S(0, T)] = T, \tag{B5}$$

respectively.

Along the characteristic lines $X = T - T_0$, $T_0 > 0$, Eq. (B4) can be transformed as follows:

$$\frac{1}{A(S)} \frac{dS}{dX} = -S. \quad (\text{B6})$$

Note that the characteristic lines $X = T - T_0$, $T_0 > 0$ cover the overall domain $T > X$. Integrating Eq. (B6) over X and imposing boundary condition (B5) yield solution $S(X, T)$ in the form (15).

Taking derivative with respect to T on both sides of Eq. (15) yields

$$\frac{1}{SA(S)} \frac{\partial S(X, T)}{\partial T} = \frac{1}{S(0, T - X)A[S(0, T - X)]} \frac{dS(0, T - X)}{dT}. \quad (\text{B7})$$

Substitution of Eq. (10) into Eq. (B7) yields

$$\frac{C(X, T)}{S(X, T)} = \frac{C(0, T - X)}{S(0, T - X)}, \quad T > X. \quad (\text{B8})$$

As it follows from Eq. (B8), the value C/S is constant along the characteristic lines $X = T - T_0$, $T_0 > 0$, i.e. C/S is Riemann invariant. Accounting for boundary condition (13) in Eq. (B8) yields formula (16) for suspension concentration in the domain $T > X$.

References

- Abdel-Salam, A., Chrysikopoulos, C.V.: Modeling of colloid and colloid-facilitated contaminant transport in a two-dimensional fracture with spatially variable aperture. *Transp. Porous Med.* **20**(3), 197–221 (1995)
- Alem, A., Ahfir, N.-D., Elkawafi, A., Wang, H.: Hydraulic operating conditions and particle concentration effects on physical clogging of a porous medium. *Transp. Porous Med.* **106**(2), 303–321 (2015)
- Alvarez, A., Bedrikovetsky, P., Hime, G., Marchesin, A., Marchesin, D., Rodrigues, J.: A fast inverse solver for the filtration function for flow of water with particles in porous media. *Inverse Probl.* **22**(1), 69 (2005)
- Alvarez, A.C., Hime, G., Marchesin, D., Bedrikovetsky, P.G.: The inverse problem of determining the filtration function and permeability reduction in flow of water with particles in porous media. *Transp. Porous Med.* **70**(1), 43–62 (2007)
- Arab, D., Pourafshary, P.: Nanoparticles-assisted surface charge modification of the porous medium to treat colloidal particles migration induced by low salinity water flooding. *Colloids Surf. A Physicochem. Eng. Asp.* **436**, 803–814 (2013)
- Arab, D., Pourafshary, P., Ayatollahi, S.: Mathematical modeling of colloidal particles transport in the medium treated by nanofluids: deep bed filtration approach. *Transp. Porous Med.* **103**(3), 401–419 (2014)
- Araújo, J.A., Santos, A.: Analytic model for DBF under multiple particle retention mechanisms. *Transp. Porous Med.* **97**(2), 135–145 (2013)
- Arns, C., Adler, P.: Fast Laplace solver approach to pore-scale permeability. *Phys. Rev. E* **97**(2), 023303 (2018)
- Bashtani, F., Taheri, S., Kantzas, A.: Scale up of pore-scale transport properties from micro to macro scale; network modelling approach. *J. Petrol. Sci. Eng.* **170**, 541–562 (2018)
- Bedrikovetsky, P.: Upscaling of stochastic micro model for suspension transport in porous media. *Transp. Porous Med.* **75**(3), 335–369 (2008)
- Bedrikovetsky, P.: *Mathematical Theory of Oil and Gas Recovery: With Applications to Ex-USSR Oil and Gas Fields*, vol. 4. Springer, Berlin (2013)
- Bedrikovetsky, P., You, Z., Badalyan, A., Osipov, Y., Kuzmina, L.: Analytical model for straining-dominant large-retention depth filtration. *Chem. Eng. J.* **330**, 1148–1159 (2017)
- Bekhit, H.M., El-Kordy, M.A., Hassan, A.E.: Contaminant transport in groundwater in the presence of colloids and bacteria: model development and verification. *J. Contam. Hydrol.* **108**(3–4), 152–167 (2009)

- Bennacer, L., Ahfir, N.-D., Alem, A., Wang, H.: Coupled effects of ionic strength, particle size, and flow velocity on transport and deposition of suspended particles in saturated porous media. *Transp. Porous Med.* **118**(2), 251–269 (2017)
- Bradford, S.A., Kim, H.N., Haznedaroglu, B.Z., Torkzaban, S., Walker, S.L.: Coupled factors influencing concentration-dependent colloid transport and retention in saturated porous media. *Environ. Sci. Technol.* **43**(18), 6996–7002 (2009)
- Bradford, S.A., Simunek, J., Bettahar, M., van Genuchten, M.T., Yates, S.R.: Modeling colloid attachment, straining, and exclusion in saturated porous media. *Environ. Sci. Technol.* **37**(10), 2242–2250 (2003)
- Bradford, S.A., Torkzaban, S., Leij, F., Šimůnek, J., van Genuchten, M.T.: Modeling the coupled effects of pore space geometry and velocity on colloid transport and retention. *Water Resour. Res.* **45**(2) (2009b)
- Chequer, L., Russell, T., Behr, A., Genolet, L., Kowollik, P., Badalyan, A., Zeinijahromi, A., Bedrikovetsky, P.: Non-monotonic permeability variation during colloidal transport: governing equations and analytical model. *J. Hydrol.* **557**, 547–560 (2017)
- Chrysikopoulos, C.V., Sotirelis, N.P., Kallithrakas-Kontos, N.G.: Cotransport of graphene oxide nanoparticles and kaolinite colloids in porous media. *Transp. Porous Med.* **119**(1), 181–204 (2017)
- Civan, F.: *Reservoir Formation Damage*. Gulf Professional Publishing, Houston (2015)
- Coleman, T.F., Li, Y.: An interior trust region approach for nonlinear minimization subject to bounds. *SIAM J. Optim.* **6**(2), 418–445 (1996)
- Elimelech, M., Gregory, J., Jia, X.: *Particle Deposition and Aggregation: Measurement, Modelling and Simulation*. Butterworth-Heinemann, Oxford (2013)
- Farajzadeh, R., Guo, H., van Winden, J., Bruining, J.: Cation exchange in the presence of oil in porous media. *ACS Earth Space Chem.* **1**(2), 101–112 (2017)
- Guedes, R.G., Al-Abduwani, F., Bedrikovetsky, P., Currie, P.: Injectivity decline under multiple particle capture mechanisms. *J. Soc. Pet. Eng.* **14**, 477–487 (2009)
- Hammadi, A., Ahfir, N.-D., Alem, A., Wang, H.: Effects of particle size non-uniformity on transport and retention in saturated porous media. *Transp. Porous Med.* **118**(1), 85–98 (2017)
- Hayek, M.: Exact solutions for one-dimensional transient gas flow in porous media with gravity and Klinkenberg effects. *Transp. Porous Med.* **107**(2), 403–417 (2015)
- Hayek, M., Kosakowski, G., Jakob, A., Churakov, S.V.: A class of analytical solutions for multidimensional multispecies diffusive transport coupled with precipitation-dissolution reactions and porosity changes. *Water Resour. Res.* **48**(3) (2012)
- Herzig, J., Leclerc, D., Goff, P.L.: Flow of suspensions through porous media—application to deep filtration. *Ind. Eng. Chem.* **62**(5), 8–35 (1970)
- Katzourakis, V.E., Chrysikopoulos, C.V.: Mathematical modeling of colloid and virus cotransport in porous media: application to experimental data. *Adv. Water Resour.* **68**, 62–73 (2014)
- Katzourakis, V.E., Chrysikopoulos, C.V.: Modeling dense-colloid and virus cotransport in three-dimensional porous media. *J. Contam. Hydrol.* **181**, 102–113 (2015)
- Kuhnen, F., Barmettler, K., Bhattacharjee, S., Elimelech, M., Kretzschmar, R.: Transport of iron oxide colloids in packed quartz sand media: monolayer and multilayer deposition. *J. Colloid Interface Sci.* **231**(1), 32–41 (2000)
- Kuzmina, L.I., Osipov, Y.V., Galaguz, Y.P.: A model of two-velocity particles transport in a porous medium. *Int. J. Non Linear Mech.* **93**, 1–6 (2017)
- Mansouri, M., Nakhae, A., Pourafshary, P.: Effect of SiO₂ nanoparticles on fines stabilization during low salinity water flooding in sandstones. *J. Petrol. Sci. Eng.* **174**, 637–648 (2019)
- Mikhailov, D., Zhvick, V., Ryzhikov, N., Shako, V.: Modeling of rock permeability damage and repairing dynamics due to invasion and removal of particulate from drilling fluids. *Transp. Porous Med.* **121**(1), 37–67 (2018)
- Mirabolghasemi, M., Prodanović, M., DiCarlo, D., Ji, H.: Prediction of empirical properties using direct pore-scale simulation of straining through 3D microtomography images of porous media. *J. Hydrol.* **529**, 768–778 (2015)
- Oladyshkin, S., Panfilov, M.: Streamline splitting between thermodynamics and hydrodynamics in a compositional gas–liquid flow through porous media. *C. R. Méc.* **335**(1), 7–12 (2007)
- Polyanin, A.: *EqWorld, The World of Mathematical Equations*. <http://eqworld.ipmnet.ru/> (2004). Accessed 01/06/2018
- Polyanin, A., Zaitsev, V.: *Handbook of Nonlinear Partial Differential Equations*. CRC Press, Boca Raton (2012)
- Polyanin, A.D., Dil'man, V.V.: *Methods of Modeling Equations and Analogies in Chemical Engineering*. CRC Press, Boca Raton (1994)
- Polyanin, A.D., Manzhirov, A.V.: *Handbook of Mathematics for Engineers and Scientists*. CRC Press, Boca Raton (2006)

- Rottman, J., Sierra-Alvarez, R., Shadman, F.: Real-time monitoring of nanoparticle retention in porous media. *Environ. Chem. Lett.* **11**(1), 71–76 (2013)
- Russell, T., Pham, D., Neishaboob, M.T., Badalyan, A., Behr, A., Genolet, L., Kowollik, P., Zeinijahromi, A., Bedrikovetsky, P.: Effects of kaolinite in rocks on fines migration. *J. Nat. Gas Sci. Eng.* **45**, 243–255 (2017)
- Santos, A., Bedrikovetsky, P.: A stochastic model for particulate suspension flow in porous media. *Transp. Porous Med.* **62**(1), 23–53 (2006)
- Sefrioui, N., Ahmadi, A., Omari, A., Bertin, H.: Numerical simulation of retention and release of colloids in porous media at the pore scale. *Colloids Surf. A Physicochem. Eng. Asp.* **427**, 33–40 (2013)
- Shampine, L.: Solving hyperbolic PDEs in MATLAB. *Appl. Numer. Anal. Comput. Math.* **2**(3), 346–358 (2005a)
- Shampine, L.F.: Two-step Lax–Friedrichs method. *Appl. Math. Lett.* **18**(10), 1134–1136 (2005b)
- Shapiro, A., Wesselingh, J.: Gas transport in tight porous media: gas kinetic approach. *Chem. Eng. J.* **142**(1), 14–22 (2008)
- Shapiro, A., Yuan, H.: Application of stochastic approaches to modelling suspension flow in porous media. In: Skogseid, A., Fasano, V. (eds.) *Statistical Mechanics and Random Walks: Principles, Processes and Applications*. Hauppauge, New York (2012)
- Shapiro, A.A., Bedrikovetsky, P.G., Santos, A., Medvedev, O.O.: A stochastic model for filtration of particulate suspensions with incomplete pore plugging. *Transp. Porous Med.* **67**(1), 135–164 (2007)
- Shapiro, A., Bedrikovetsky, P.: Elliptic random-walk equation for suspension and tracer transport in porous media. *Phys. A: Stat. Mech. Appl.* **387**(24), 5963–5978 (2008)
- Shapiro, A., Bedrikovetsky, P.: A stochastic theory for deep bed filtration accounting for dispersion and size distributions. *Phys. A: Stat. Mech. Appl.* **389**, 2473–2494 (2010)
- Sharma, M., Yortsos, Y.: Transport of particulate suspensions in porous media: model formulation. *AIChE J.* **33**(10), 1636–1643 (1987)
- Shikhov, I., Arns, C.H.: Evaluation of capillary pressure methods via digital rock simulations. *Transp. Porous Med.* **107**(2), 623–640 (2015)
- Sorbie, K., Stamatiou, A.: Analytical solutions of a one-dimensional linear model describing scale inhibitor precipitation treatments. *Transp. Porous Med.* **123**, 271–287 (2018)
- Sotirelis, N.P., Chrysikopoulos, C.V.: Heteroaggregation of graphene oxide nanoparticles and kaolinite colloids. *Sci. Total Environ.* **579**, 736–744 (2017)
- Syngouna, V.I., Chrysikopoulos, C.V., Kokkinos, P., Tselepi, M.A., Vantarakis, A.: Cotransport of human adenoviruses with clay colloids and TiO₂ nanoparticles in saturated porous media: effect of flow velocity. *Sci. Total Environ.* **598**, 160–167 (2017)
- Wang, Y., Arns, C.H., Rahman, S.S., Arns, J.-Y.: Porous structure reconstruction using convolutional neural networks. *Math. Geosci.* **50**, 1–19 (2018a)
- Wang, Y., Rahman, S.S., Arns, C.H.: Super resolution reconstruction of μ -CT image of rock sample using neighbour embedding algorithm. *Phys. A: Stat. Mech. Appl.* **493**, 177–188 (2018b)
- Yanici, S., Arns, J.-Y., Cinar, Y., Pinczewski, W., Arns, C.: Percolation effects of grain contacts in partially saturated sandstones: deviations from Archie’s law. *Transp. Porous Med.* **96**(3), 457–467 (2013)
- You, Z., Bedrikovetsky, P., Badalyan, A., Hand, M.: Particle mobilization in porous media: temperature effects on competing electrostatic and drag forces. *Geophys. Res. Lett.* **42**(8), 2852–2860 (2015)
- Yuan, B., Moghanloo, R.G.: Analytical model of well injectivity improvement using nanofluid preflush. *Fuel* **202**, 380–394 (2017). <https://doi.org/10.1016/j.fuel.2017.04.004>
- Yuan, B., Moghanloo, R.G., Zheng, D.: Analytical evaluation of nanoparticle application to mitigate fines migration in porous media. *SPE J.* **21**(06), 2–317 (2016a)
- Yuan, B., Wang, W., Moghanloo, R.G., Su, Y., Wang, K., Jiang, M.: Permeability reduction of berea cores owing to nanoparticle adsorption onto the pore surface: mechanistic modeling and experimental work. *Energy Fuels* **31**(1), 795–804 (2016b)
- Yuan, H., Shapiro, A., You, Z., Badalyan, A.: Estimating filtration coefficients for straining from percolation and random walk theories. *Chem. Eng. J.* **210**, 63–73 (2012)
- Yuan, H., Shapiro, A.A.: Modeling non-Fickian transport and hyperexponential deposition for deep bed filtration. *Chem. Eng. J.* **162**(3), 974–988 (2010)
- Zhang, H., Malgaresi, G.V.C., Bedrikovetsky, P.: Exact solutions for suspension-colloidal transport with multiple capture mechanisms. *Int. J. Non Linear Mech.* **105**, 27–42 (2018)